Physics and Astronomy Reports
PAR 2023, 1 (2), 54–64
DOI: 10.26650/PAR.2023.00007

RESEARCH ARTICLE

An Updated Line List for Spectroscopic Investigation of G Stars- I: Redetermination of the Abundances in the Solar Photosphere

T. Şahin[1*], M. Marışmak[1], N. Çınar[1], and S. Bilir[2]

[1] Akdeniz University, Faculty of Science, Department of Space Sciences and Technologies, 07058, Antalya, Turkiye
[2] Istanbul University, Faculty of Science, Department of Astronomy and Space Sciences, 34119, Beyazit, Istanbul, Turkiye

ABSTRACT
We propose a line list that may be useful for the abundance analysis of G-type stars in the wavelength range 4080 – 6780 Å. It is expected that the line list will be useful for surveys/libraries with overlapping spectral regions (e.g. ELODIE/SOPHIE libraries, UVES-580 setting of *Gaia*-ESO), and in particular for the analysis of F- and G-type stars in general. The atomic data are supplemented by detailed references to the sources. We estimated the Solar abundances using stellar lines and the high-resolution Kitt Peak National Observatory (KPNO) spectra of the Sun to determine the uncertainty in the log gf values. By undertaking a systematic search that makes use of the lower excitation potential and gf-values and using revised multiplet table as an initial guide, we identified 363 lines of 24 species that have accurate gf-values and are free of blends in the spectra of the Sun and a Solar analogue star, HD 218209 (G6V), for which accurate and up-to-date abundances were obtained from both ELODIE and PolarBASE spectra of the star. For the common lines with the *Gaia*-ESO line list v.6 provided by the *Gaia*-ESO collaboration, we discovered significant inconsistencies in the gf-values for certain lines of varying species.

Keywords: Line: identification; Sun: abundances; Sun: fundamental parameters; Stars: individual (HD 218209)

1. INTRODUCTION

Mid-spectral type main-sequence stars (F and G-type stars) play a significant role in understanding the Galactic chemical evolution and history of Galactic structure. These stars formed in the early Milky Way or are currently forming, have main-sequence lifetimes comparable to the age of the Galaxy. F and G-type main-sequence stars have an internal structure consisting of a radiative core surrounded by a large envelope. Such structural configuration prevents heavy elements produced in the core from mixing into the stellar atmosphere. Consequently, mid-spectral type stars carry the chemical composition of the molecular cloud in which they were born. The study of the abundances of heavy elements detected in the atmospheres of F and G-type stars provides valuable insights into the Galactic chemical evolution and the history of Galactic structure, as noted by Pagel & Patchett (1975).

Moreover, these stars offer crucial information about the formation of different populations within the Galaxy, including the halo, thick disc, and thin disc. By analyzing the kinematics and orbital dynamics of stars that have been spectroscopically studied, one can distinguish between these different population groups in the Milky Way. In addition to providing insights into Galactic chemical evolution and the formation of the Galaxy, considering the case for pure spectroscopic analysis, for instance, the α-element abundances determined through spectroscopic analysis of stars play a crucial role in testing the population membership of host galaxies.

The abundance of elements in a stellar spectrum, such as metallicity ([Fe/H]), can also be used to estimate the age of the star. This is because the youngest stars have relatively higher metal abundances and metallicity compared to the oldest stars (Placco et al. 2021). Therefore, pure spectroscopic analysis alone provides crucial information about the nature of host galaxies, in addition to insights into the age and chemical composition of individual stars.

The kinematics, orbital dynamics, and chemical properties of stars are not only the key in understanding the chemical structure of our Galaxy and its accompanying formation scenarios but also in determining the origins of (metal-poor) young and old G-spectral type stars. In this context, the author's research team is currently engaged in a thorough investigation encompassing more than 90 G-type metal-poor stars residing within the Solar neighbourhood. This study aims to investigate the origins of these stars by analyzing their kinematics, orbital dynamics, and chemical properties. This research will shed light on the formation processes and evolutionary pathways of metal-poor G spectral-type stars in our Galaxy.

Furthermore, the author's group has previously conducted a

Corresponding Author: Timur Şahin **E-mail:** timursahin@akdeniz.edu.tr
Submitted: 16.08.2023 • **Revision Requested:** 15.09.2023 • **Last Revision Received:** 10.10.2023 • **Accepted:** 13.10.2023

thorough investigation of six metal-poor F-type dwarf stars in the Solar neighbourhood, with [Fe/H] values ranging from −2.4 to −1 dex. It is worth noting that the studied metal-poor F-type dwarf stars exhibited significant changes in model atmosphere parameters (effective temperature, $T_{\rm eff}$; surface gravity, $\log g$; metallicity, [Fe/H]; microturbulence, ξ), as reported in the literature. This research, as published in Şahin & Bilir (2020), employed state-of-the-art analysis methods, including classical spectroscopy with the help of ELODIE spectra. By combining these analysis techniques, the authors were able to determine the Galactic origin of these F-type dwarf stars in the Solar neighbourhood.

The determination of accurate metal abundances depends on the accurate determination of model parameters. Current spectroscopic sky survey programs for metal-poor late spectral stars, for example, indicate the need to determine precisely calibrated model parameters for them. These current sky survey programs include *Gaia*-ESO Public Spectroscopic Survey (GES; Gilmore et al. 2012), GALactic Archaeology with HERMES (GALAH; Heijmans et al. 2012; De Silva et al. 2015; Martell et al. 2017), the Large Sky Area Multi-Object Fiber Spectroscopic Telescope (LAMOST; Zhao et al. 2012), the Sloan Extension for Galactic Understanding and Exploration (SEGUE; Yanny et al. 2009), the Apache Point Observatory Galactic Evolution Experiment (APOGEE; Allende Prieto et al. 2008), and the RAdial Velocity Experiment (RAVE; Steinmetz et al. 2006), and demonstrate that precisely determined and calibrated model atmosphere parameters are required in different regions of the electromagnetic spectrum due to differences in adopted observational methods and techniques in these surveys, for which reliable line lists and atomic data are required.

In this study, we present an up-to-date line list for planned spectral analyses in the framework of the comprehensive study mentioned above. HD 218209 of G6V, the most metal-rich star among 90 G spectral-type program stars ($-2.5 <$ [Fe/H] (dex) < -0.5), was selected for the preparation of the line list which is expected to be useful for the surveys/libraries with overlapping spectral regions (e.g. ELODIE library; Soubiran et al. 2003) and for the analysis of F and G-type stars in general.

This paper is organized as follows. Section 2 provides information concerning the observations. Section 3 explains the procedures used to measure and identify lines, as well as the techniques employed to determine the model parameters and conduct chemical abundance analyses of both HD 218209 and the Sun. Section 4 is dedicated to discussing findings and their potential implications.

2. OBSERVATIONS

For the creation of the line list in this study, high resolution ($R \approx 42\,000$) and high signal to noise (S/N = 165 at 550 nm) ELODIE spectrum (HJD 2451184.23521; $R \approx 42\,000$; exposure time 1800 s) of HD 218209 was selected. The ELODIE cross-dispersed echelle spectrograph provided spectral coverage from 3900 to 6800 Å. The spectrum was continuum normalized and wavelength calibrated, and the radial velocity (RV) was corrected by the data reduction pipeline at the telescope. Since some problems were encountered in the continuum normalization of the spectra from the library, the spectrum was renormalized.

Since high resolution ($R \approx 76\,000$) and high signal to noise (S/N = 140 at 550 nm) PolarBASE[1] (Petit et al. 2014) Narval[2] spectrum (HJD 2456232.48238; exposure time 400 s) of the star was also available, it was used to test model parameters for the star. Prior to the line measurement process, the PolarBASE spectrum was also renormalized and corrected for the radial velocity (RV). For RV correction, we used a Python interface and the NARVAL atomic line library containing atomic transitions from 4000 to 6800 Å. For renormalization, we used an in-house developed interactive normalization code LIME (Şahin 2017) in Interactive Data Language (IDL) prior to the abundance analysis.

The Solar spectrum is certainly a primary reference for stellar astrophysics and for interpreting physical processes in stars (Molaro & Monai 2012). The high-resolution ($R \approx 400\ 000$) spectrum of the Sun used in this study was obtained with the Kitt Peak Fourier Transform Spectrometer (FTS; Kurucz et al. 1984). The character of the spectra of HD 218209 and the Sun is displayed in Figure 1.

3. THE ABUNDANCE ANALYSIS

We employed ATLAS9 model atmospheres (Castelli & Kurucz 2003) computed in local thermodynamic equilibrium (LTE) with NEWODF opacities for the abundance study of HD 218209 and the Solar spectrum. Elemental abundances were computed by using the LTE line analysis code MOOG (Sneden 1973)[3]. The details of the abundance analysis and the source of the atomic data are the same as in Şahin & Lambert (2009), Şahin et al. (2011, 2016) and Şahin & Bilir (2020). The line list, atomic data, and model parameter derivation are covered in the following subsections.

3.1. Line List: Line Measurement, Identification and Atomic Data

An essential prerequisite for abundance analysis of a star is a set of identified lines with reliable atomic data. Our line lists were created by a systematic search for unblended lines (useful for equivalent width–EW– analysis technique). For line measurement from the ELODIE spectrum of HD 218209, a systematic

[1] http://polarbase.irap.omp.eu
[2] Narval spectropolarimeter is adapted to the 2m Bernard Lyot telescope and provides high-resolution spectral and polarimetric data.
[3] The MOOG source code is available at http://www.as.utexas.edu/chris/moog.html

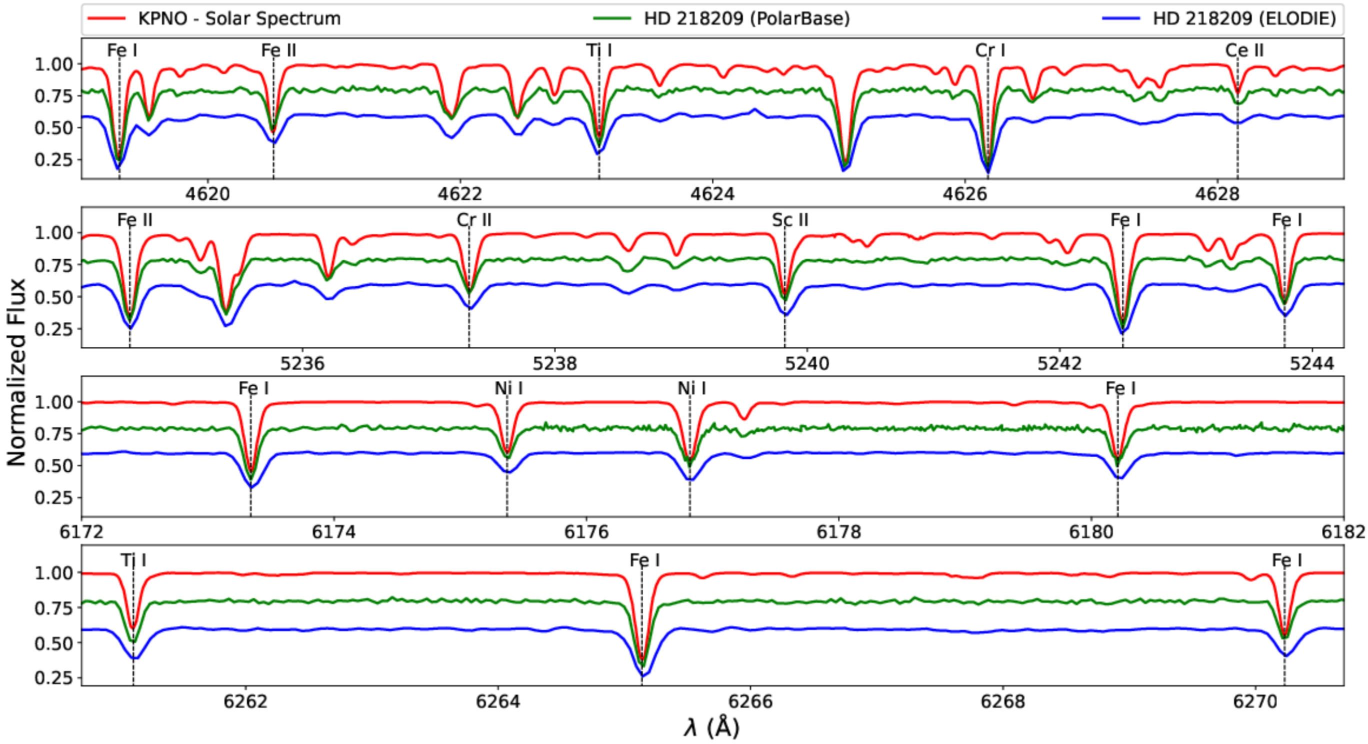

Figure 1. A small region of the KPNO, PolarBASE, and ELODIE spectra of HD 218209 and the Sun. Identified lines are also indicated.

search for unblended lines was performed. The line centre positions were measured in several segments, each containing a portion of the spectra of 20 Å. For this, the LIME (Şahin 2017) code was employed. The code provides a list of possible transitions in the close neighbourhood of the measured line together with recent atomic data (e.g. Rowland Multiplet Number-RMT, $\log gf$, and lower Level Excitation Potential-LEP) that are compiled from the literature (e.g. from NIST database). The MOORE catalogue (Moore et al. 1966) was configured as one of the reference atomic line libraries in the LIME code. Following the line identification step, a multiplet analysis technique was performed to assess whether the detected lines belong to the candidate element indicated by the code. Our final list covers 24 species and 363 lines over the spectrum range from about 4100 – 6800 Å. The identified lines have accurate gf-values and are free of blends in the spectra of the Sun and HD 218209. The number of identified lines in the respective wavelength regions of the KPNO Solar spectrum is presented in Figure 2. Our selection of iron lines included 132 Fe I lines with excitation potentials (LEPs) ranging from 0.05 to ≈5 eV and 17 Fe II lines. Chosen lines of Fe I and Fe II are exhibited in Table 1. In Table 2, we provide the list of identified lines other than iron with the atomic data, their measured equivalent widths (obtained using the LIME code) and computed logarithmic abundances in the Solar spectrum and in the spectrum of HD 218209.

3.2. Model Parameters and Abundances

We used neutral and ionised Fe lines to determine model atmospheric parameters such as effective temperature, surface gravity, microturbulence, and metallicity (Table 5). First, the effective temperature was calculated by requiring that the resulting abundance be independent of the lower LEP.

If all lines have the same LEP and a similar wavelength, the microturbulence (ξ) is determined by requiring that the calculated abundance be independent of the reduced equivalent width (EW). The precision in the determination of the microturbulent velocity is ±0.5 km s^{-1}. We determined the surface gravity ($\log g$) by ensuring ionization equilibrium, which requires that the Fe I and Fe II lines yield the same iron abundance. (Figures 3 and 4). Due to the interdependence of model parameters, an iterative procedure is required. Between each of the above steps, minor adjustments are made to the model parameters. We also confirmed that there is no substantial trend in iron abundances (see Figures 3 and 4 for the Sun and HD 218209, respectively).

The model parameters obtained for the Sun as a result of the Solar analysis were determined as $T_{\rm eff}$ = 5790 K, $\log g$ = 4.4 cgs, [Fe/H]=0 dex and ξ = 0.66 km s^{-1}. These values are similar to those recommended by Heiter et al. (2015) as ($T_{\rm eff}$, $\log g$) = (5771, 4.438). Element abundances for the Sun were calculated with these model parameters. For HD 218209, the model parameters were obtained from ELODIE and PolarBASE spectrum of the star.

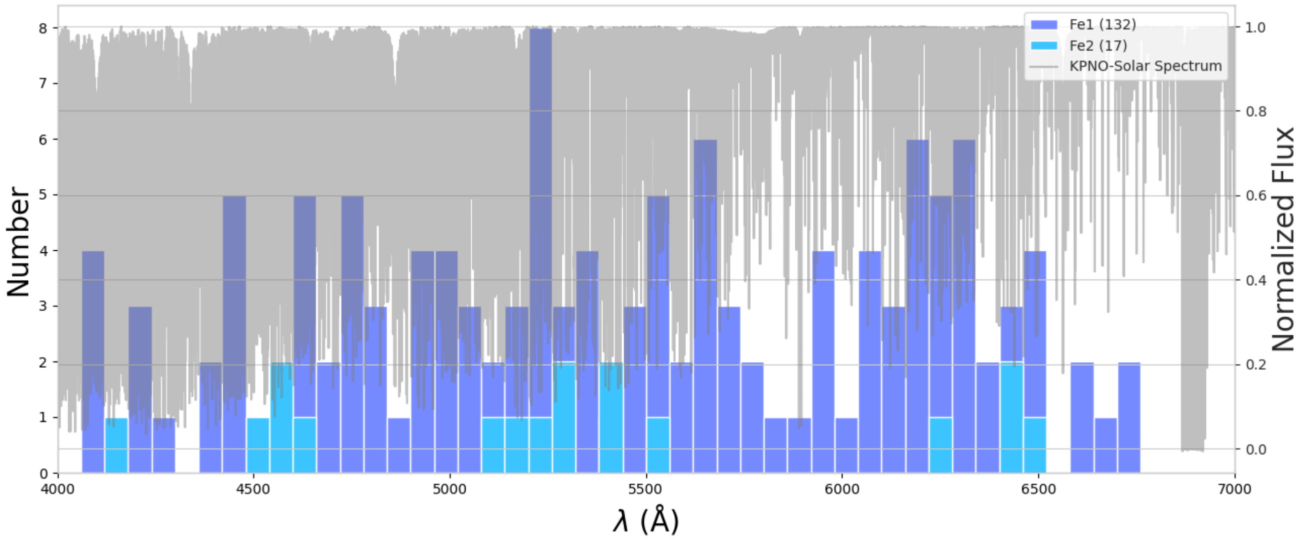

Figure 2. The KPNO Solar spectrum and the number of identified lines in the respective wavelength regions (each bar indicates 50 Å region of the spectrum).

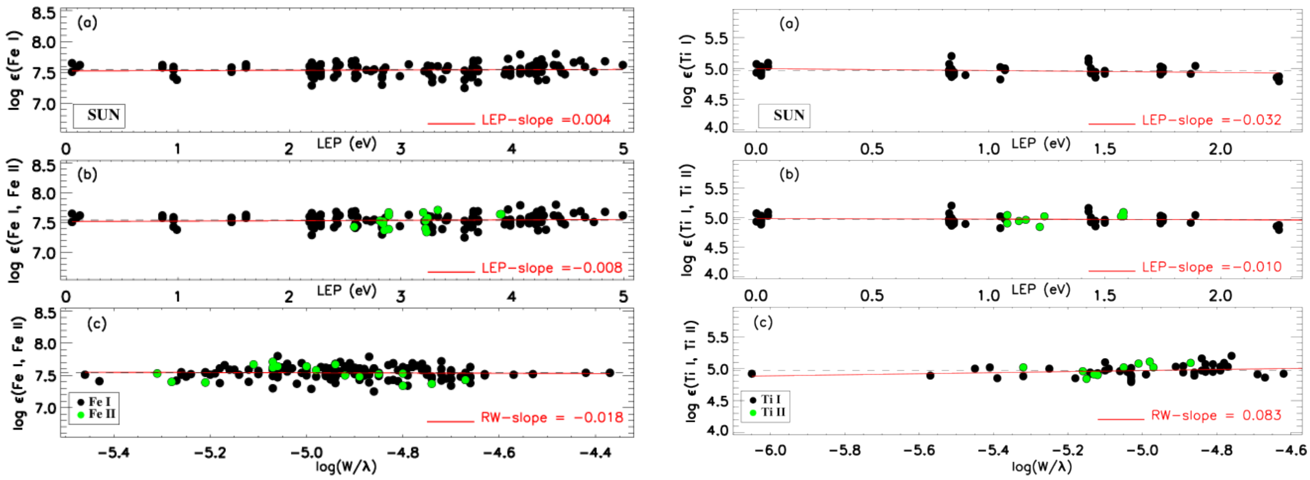

Figure 3. An example for the determination of the atmospheric parameters $T_{\rm eff}$ and ξ using abundance (log ϵ) as a function of both lower LEP (panels a and b for Fe and Ti, respectively) and reduced EW (REW; log (EW/λ), panels c for Fe and Ti, respectively) for the Sun. In all panels, the solid red line represents the least-squares fit to the data.

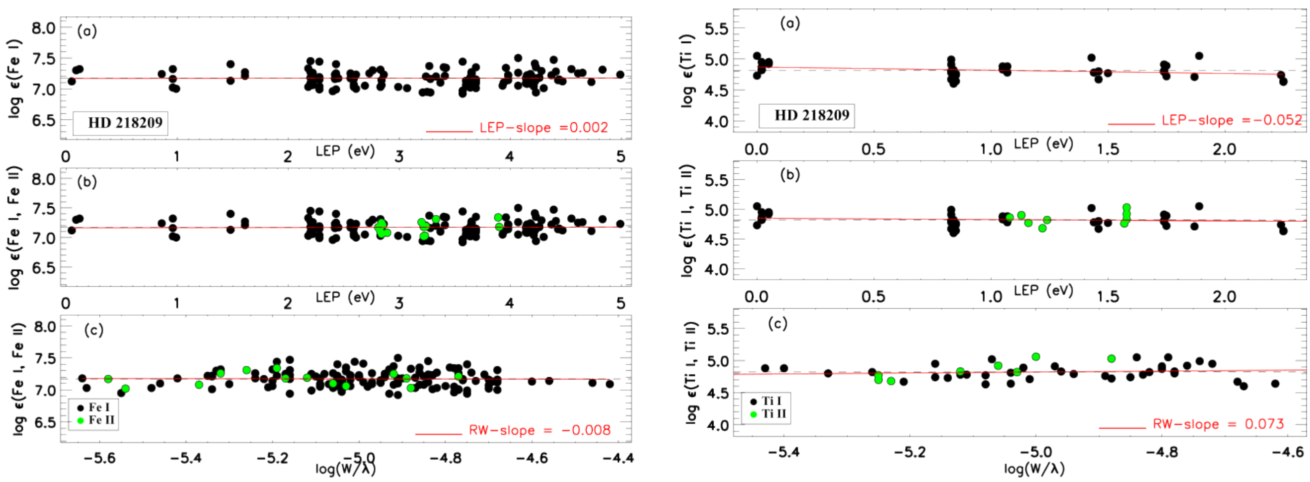

Figure 4. An example for the determination of the atmospheric parameters $T_{\rm eff}$ and ξ using abundance (log ϵ) as a function of both lower LEP (panels a and b for Fe and Ti, respectively) and reduced EW (REW; log (EW/λ), panels c for Fe and Ti, respectively) for HD 218209 and the ELODIE spectrum. In all panels, the solid red line represents the least-squares fit to the data.

Table 1. Fe I and Fe II lines. The abundances are obtained for a model of $T_{\rm eff}$ = 5790 K, log g = 4.4 cgs, and ξ = 0.66 km s^{-1}.

Spec.	λ (Å)	LEP (eV)	log(gf) (dex)	Sun EW (mÅ)	Sun log ϵ(X) (dex)	HD 218209 EW (mÅ)	HD 218209 log ϵ(X) (dex)	RMT	Spec.	λ (Å)	LEP (eV)	log(gf) (dex)	Sun EW (mÅ)	Sun log ϵ(X) (dex)	HD 218209 EW (mÅ)	HD 218209 log ϵ(X) (dex)	RMT
Fe I	4080.22	3.28	-1.23	80.9	7.34	85.1	7.16	558	Fe I	5618.64	4.21	-1.28	49.3	7.47	34.3	7.04	1107
Fe I	4082.11	3.42	-1.51	72.7	7.60	69.8	7.34	698	Fe I	5624.03	4.39	-1.20*	49.2	7.55	38.9	7.22	1160
Fe I	4088.56	3.64	-1.50	52.4	7.43	43.9	7.09	906	Fe I	5633.95	4.99	-0.32	67.3	7.62	53.2	7.23	1314
Fe I	4090.96	3.37	-1.73	55.5	7.39	49.9	7.10	700	Fe I	5636.71	3.64	-2.56	19.6	7.51	13.0	7.18	868
Fe I	4204.00	2.84	-1.01	125.1	7.52	115.9	7.14	355	Fe I	5638.27	4.22	-0.84	75.4	7.54	61.1	7.12	1087
Fe I	4207.13	2.83	-1.41	83.5	7.44	88.1	7.31	352	Fe I	5641.45	4.26	-1.15	66.0	7.71	45.4	7.18	1087
Fe I	4220.35	3.07	-1.31	91.4	7.63	70.9	7.01	482	Fe I	5662.52	4.18	-0.57	92.4	7.61	81.1	7.24	1087
Fe I	4291.47	0.05	-4.08	92.3	7.51	87.1	7.12	3	Fe I	5701.56	2.56	-2.22	87.1	7.68	70.6	7.17	209
Fe I	4365.90	2.99	-2.25	49.2	7.44	38.1	7.03	415	Fe I	5705.47	4.30	-1.36	37.5	7.38	25.8	7.01	1087
Fe I	4389.25	0.05	-4.58	75.4	7.65	63.9	7.12	2	Fe I	5717.84	4.28	-1.10	63.3	7.62	53.8	7.29	1107
Fe I	4432.58	3.57	-1.56	51.4	7.38	40.2	6.97	797	Fe I	5741.86	4.26	-1.67	31.5	7.51	21.8	7.18	1086
Fe I	4439.89	2.28	-3.00	48.4	7.49	34.4	6.99	116	Fe I	5778.46	2.59	-3.43	21.5	7.41	13.6	7.03	209
Fe I	4442.35	2.20	-1.25	187.7	7.54	167.6	7.09	68	Fe I	5806.73	4.61	-1.03	56.4	7.69	39.7	7.25	1180
Fe I	4447.14	2.20	-2.73	66.2	7.66	64.1	7.45	69	Fe I	5916.26	2.45	-2.99	54.5	7.62	40.7	7.17	170
Fe I	4447.73	2.22	-1.34	171.0	7.54	155.7	7.11	68	Fe I	5929.68	4.55	-1.38	39.7	7.66	28.6	7.32	1176
Fe I	4502.60	3.57	-2.31	28.9	7.53	29.1	7.44	796	Fe I	5934.67	3.93	-1.12	76.6	7.47	61.7	7.05	982
Fe I	4556.93	3.25	-2.66	25.9	7.48	12.7	6.95	638	Fe I	5952.73	3.98	-1.39	59.6	7.50	53.0	7.22	959
Fe I	4593.53	3.94	-2.03	28.3	7.54	16.1	7.10	971	Fe I	5956.71	0.86	-4.61	52.8	7.62	–	–	14
Fe I	4602.01	1.61	-3.15	72.0	7.58	64.8	7.21	39	Fe I	6027.06	4.07	-1.09	62.7	7.48	48.8	7.05	1018
Fe I	4602.95	1.48	-2.22	122.5	7.51	116.3	7.13	39	Fe I	6065.49	2.61	-1.53	118.5	7.45	102.9	7.00	207
Fe I	4619.30	3.60	-1.08	84.1	7.45	73.7	7.06	821	Fe I	6079.02	4.65	-1.10	45.6	7.59	34.8	7.26	1176
Fe I	4630.13	2.28	-2.59	72.7	7.63	61.9	7.19	115	Fe I	6082.72	2.22	-3.57	35.2	7.52	28.1	7.21	64
Fe I	4635.85	2.84	-2.36	54.9	7.54	41.2	7.06	349	Fe I	6096.67	3.98	-1.88	37.5	7.55	27.2	7.22	959
Fe I	4678.85	3.60	-0.83	102.5	7.47	95.2	7.13	821	Fe I	6127.91	4.14	-1.40	48.3	7.52	37.3	7.17	1017
Fe I	4704.95	3.69	-1.53	61.5	7.55	48.6	7.12	821	Fe I	6137.70	2.59	-1.40	135.6	7.48	122.8	7.07	207
Fe I	4728.55	3.65	-1.17	81.3	7.65	69.3	7.23	822	Fe I	6157.73	4.07	-1.22	61.0	7.56	53.2	7.26	1015
Fe I	4733.60	1.48	-2.99	82.9	7.58	84.8	7.40	38	Fe I	6165.36	4.14	-1.47	44.6	7.51	30.7	7.09	1018
Fe I	4735.85	4.07	-1.32	64.1	7.79	57.6	7.50	1042	Fe I	6173.34	2.22	-2.88	68.9	7.61	58.6	7.22	62
Fe I	4741.53	2.83	-1.76	72.6	7.41	63.5	7.03	346	Fe I	6180.21	2.73	-2.65	53.4	7.52	47.6	7.25	269
Fe I	4745.81	3.65	-1.27	78.2	7.69	66.2	7.27	821	Fe I	6200.32	2.61	-2.44	71.5	7.59	62.6	7.23	207
Fe I	4788.77	3.24	-1.76	65.6	7.61	55.0	7.20	588	Fe I	6213.44	2.22	-2.48	82.5	7.50	75.6	7.18	62
Fe I	4802.89	3.64	-1.51	60.0	7.52	44.3	7.02	888	Fe I	6219.29	2.20	-2.43	87.9	7.54	79.1	7.18	62
Fe I	4839.55	3.27	-1.82	62.2	7.60	58.3	7.37	588	Fe I	6232.65	3.65	-1.22	81.5	7.60	71.9	7.25	816
Fe I	4875.88	3.33	-1.97	61.0	7.60	49.2	7.20	687	Fe I	6240.65	2.22	-3.17	47.6	7.40	39.1	7.06	64
Fe I	4917.23	4.19	-1.16	62.7	7.61	49.4	7.21	1066	Fe I	6252.56	2.40	-1.69	119.6	7.42	103.2	6.96	169
Fe I	4918.02	4.23	-1.34	53.0	7.63	45.5	7.35	1070	Fe I	6265.14	2.18	-2.55	86.2	7.60	82.5	7.33	62
Fe I	4924.78	2.28	-2.11	92.8	7.52	85.2	7.15	114	Fe I	6270.23	2.86	-2.61	53.0	7.58	43.1	7.23	342
Fe I	4939.69	0.86	-3.34	99.7	7.58	95.8	7.24	16	Fe I	6297.80	2.22	-2.74	73.6	7.56	67.1	7.26	62
Fe I	4961.92	3.63	-2.25	26.5	7.42	16.4	7.03	845	Fe I	6301.51	3.65	-0.72	112.7	7.57	106.2	7.26	816
Fe I	4962.58	4.18	-1.18	54.0	7.51	40.3	7.09	66	Fe I	6315.81	4.07	-1.66	39.8	7.51	–	–	1014
Fe I	4973.10	3.96	-0.92	93.8	7.72	82.4	7.34	173	Fe I	6322.69	2.59	-2.43	78.6	7.69	61	7.16	207
Fe I	5002.80	3.40	-1.53	78.8	7.54	81.2	7.35	687	Fe I	6335.34	2.20	-2.18	96.3	7.43	88.6	7.08	62
Fe I	5022.24	3.98	-0.56	99.5	7.45	93.9	7.14	965	Fe I	6336.83	3.69	-0.86	102.4	7.34	94.8	7.01	816
Fe I	5029.62	3.41	-2.00	48.7	7.54	40.0	7.21	718	Fe I	6344.15	2.43	-2.92	59.2	7.61	56.4	7.40	169
Fe I	5074.75	4.22	-0.23	118.8	7.50	105.8	7.12	1094	Fe I	6393.61	2.43	-1.58	134.6	7.48	113.4	6.99	168
Fe I	5083.35	0.96	-2.96	109.9	7.43	101.8	7.02	16	Fe I	6408.03	3.69	-1.02	97.3	7.69	88.1	7.35	816
Fe I	5088.16	4.15	-1.75	34.8	7.59	23.5	7.22	1066	Fe I	6419.96	4.73	-0.27	86.8	7.51	71.3	7.11	1258
Fe I	5141.75	2.42	-2.24	89.3	7.68	76.5	7.23	114	Fe I	6430.86	2.18	-2.01	115.3	7.51	97.9	7.03	62
Fe I	5145.10	2.20	-3.08*	52.5	7.49	49.0	7.26	66	Fe I	6469.19	4.83	-0.81	58.6	7.68	44.5	7.31	1258
Fe I	5198.72	2.22	-2.13	94.9	7.48	91.1	7.17	66	Fe I	6481.88	2.28	-2.98	64.7	7.63	62.9	7.44	109
Fe I	5217.40	3.21	-1.16	121.7	7.52	93.8	6.94	553	Fe I	6498.94	0.96	-4.69	45.7	7.59	40.9	7.32	13
Fe I	5228.38	4.22	-1.26	60.0	7.68	53.5	7.41	1091	Fe I	6518.37	2.83	-2.46†	56.0	7.46	–	–	342
Fe I	5242.50	3.63	-0.97	85.7	7.50	73.2	7.08	843	Fe I	6593.88	2.43	-2.42	83.7	7.60	75.0	7.25	168
Fe I	5243.78	4.26	-1.12	63.0	7.64	46.6	7.18	1089	Fe I	6609.12	2.56	-2.69	65.6	7.62	55.1	7.25	206
Fe I	5247.06	0.09	-4.95	65.3	7.58	61.3	7.30	1	Fe I	6678.00	2.69	-1.42	133.5	7.54	112.1	7.05	268
Fe I	5250.22	0.12	-4.94	65.9	7.62	61.5	7.32	1	Fe I	6703.58	2.76	-3.06	37.2	7.55	31.7	7.30	268
Fe I	5250.65	2.20	-2.18	100.6	7.60	95.7	7.27	66	Fe I	6750.16	2.42	-2.62	73.3	7.56	61.8	7.16	111
Fe I	5253.47	3.28	-1.57	77.9	7.42	62.2	6.94	553	Fe II	4178.86	2.58	-2.51*	89.7	7.50	77.2	7.19	28
Fe I	5288.53	3.69	-1.51	58.6	7.52	48.4	7.15	929	Fe II	4508.29	2.85	-2.44*	82.1	7.46	76.6	7.30	38
Fe I	5298.78	3.64	-2.02	42.2	7.57	30.3	7.18	875	Fe II	4576.34	2.84	-2.92	65.3	7.52	54.8	7.25	38
Fe I	5307.37	1.61	-2.99	87.6	7.63	80.3	7.27	36	Fe II	4582.83	2.84	-3.06	58.6	7.48	42.8	7.06	37
Fe I	5322.05	2.28	-2.80	59.4	7.44	48.9	7.04	112	Fe II	4620.52	2.83	-3.19	55.3	7.50	39.8	7.10	38
Fe I	5365.41	3.57	-1.22*	74.4	7.45	66.3	7.12	786	Fe II	5132.67	2.81	-4.09	25.1	7.53	13.6	7.17	35
Fe I	5373.71	4.47	-0.84	61.1	7.47	49.5	7.12	1166	Fe II	5197.58	3.23	-2.22*	81.6	7.51	68.3	7.20	49
Fe I	5379.58	3.69	-1.51	59.7	7.53	46.1	7.09	928	Fe II	5234.63	3.22	-2.21	83.8	7.53	68.2	7.18	49
Fe I	5398.29	4.44	-0.71	71.1	7.50	60.3	7.15	553	Fe II	5264.81	3.33	-3.13*	45.2	7.61	29.0	7.21	48
Fe I	5473.91	4.15	-0.79	78.2	7.49	65.1	7.08	1062	Fe II	5284.11	2.89	-3.11*	61.1	7.58	–	–	41
Fe I	5483.11	4.15	-1.41	46.2	7.49	–	–	1061	Fe II	5414.07	3.22	-3.58*	28.6	7.50	15.5	7.12	48
Fe I	5487.15	4.41	-1.51	36.5	7.61	26.3	7.28	1143	Fe II	5425.26	3.20	-3.22*	42.5	7.50	26.2	7.09	49
Fe I	5501.48	0.96	-3.05	116.6	7.54	109.8	7.16	15	Fe II	5534.85	3.24	-2.75*	58.3	7.48	41.7	7.08	55
Fe I	5506.79	0.99	-2.80	121.6	7.38	115.1	7.00	15	Fe II	6247.56	3.89	-2.30*	54.1	7.51	40.6	7.21	74
Fe I	5525.55	4.23	-1.08	53.3	7.37	38.1	6.94	1062	Fe II	6432.68	2.89	-3.57*	40.1	7.46	27.5	7.15	40
Fe I	5543.94	4.22	-1.11	62.2	7.57	48.9	7.17	1062	Fe II	6456.39	3.90	-2.05*	64.6	7.50	43.9	7.04	74
Fe I	5546.51	4.37	-1.28	49.7	7.62	35.8	7.22	1145	Fe II	6516.08	2.89	-3.31*	54.9	7.56	–	–	40
Fe I	5560.22	4.43	-1.16	50.2	7.56	35.4	7.14	1164									

Table 2. Lines used in the analysis of the KPNO Solar spectrum and HD 218209. Abundances for individual lines are those obtained for a model of $T_{\rm eff}$ = 5790 K, log g = 4.4 cgs, and ξ = 0.66 km s^{-1}.

Spec.	λ (Å)	LEP (eV)	log(gf) (dex)	Sun EW (mÅ)	Sun log ϵ(X) (dex)	HD 218209 EW (mÅ)	HD 218209 log ϵ(X) (dex)	RMT	Ref.	Spec.	λ (Å)	LEP (eV)	log(gf) (dex)	Sun EW (mÅ)	Sun log ϵ(X) (dex)	HD 218209 EW (mÅ)	HD 218209 log ϵ(X) (dex)	RMT	Ref.
Na I	5682.65	2.10	-0.67	100.1	6.21	82.4	5.86	6	1	Ti I	5145.47	1.46	-0.54	37.2	4.94	31.4	4.67	109	7
Na I	5688.22	2.10	-0.37	121.1	6.11	99.9	5.72	6	1	Ti I	5147.48	0.00	-1.94	38.8	4.93	37.7	4.73	4	7
Mg I	4571.10	0.00	-5.40	109.2	7.54	115.1	7.44	1	2	Ti I	5152.19	0.02	-1.95	36.9	4.92	–	–	4	7
Mg I	5711.10	4.34	-1.74	104.6	7.65	107.6	7.52	8	2	Ti I	5192.98	0.02	-0.95	84.0	5.03	85.2	4.83	4	7
Si I	5645.62	4.93	-2.03	35.5	7.50	–	–	10	3	Ti I	5210.39	0.05	-0.82	89.0	5.03	98.6	4.95	4	7
Si I	5665.56	4.92	-1.99	39.6	7.53	31.0	7.37	10	3	Ti I	5219.71	0.02	-2.22	29.1	5.00	29.0	4.82	4	7
Si I	5684.49	4.95	-1.58	60.6	7.52	54.3	7.35	11	3	Ti I	5490.16	1.46	-0.84	22.4	4.85	25.6	4.80	3	7
Si I	5708.40	4.95	-1.47	74.7	7.64	62.2	7.37	10	4	Ti I	5866.46	1.07	-0.79	46.9	4.97	44.9	4.78	72	7
Si I	5772.15	5.08	-1.62	52.0	7.53	40.0	7.27	17	3	Ti I	6126.22	1.07	-1.42	21.7	5.00	23.0	4.88	69	7
Si I	5793.08	4.93	-1.86	42.4	7.46	31.6	7.20	9	3	Ti I	6258.11	1.44	-0.39	51.4	5.00	48.3	4.78	104	7
Si I	5948.54	5.08	-1.09	83.8	7.51	–	–	16	3	Ti I	6261.11	1.43	-0.53	49.9	5.10	53.2	5.02	104	7
Si I	6125.03	5.61	-1.53	30.9	7.51	23.1	7.31	30	3	Ti I	6336.11	1.44	-1.69	5.60	4.92	–	–	103	7
Si I	6142.49	5.62	-1.48	33.3	7.51	26.8	7.35	30	3	Ti I	6743.13	0.90	-1.63	18.0	4.89	–	–	48	7
Si I	6145.02	5.61	-1.39	37.9	7.50	27.6	7.26	29	3	Ti II	4443.81	1.08	-0.71	139.7	5.04	139.9	4.86	19	7
Si I	6244.48	5.61	-1.29	44.0	7.51	32.9	7.27	27	3	Ti II	4468.50	1.13	-0.63	134.1	4.94	149.8	4.90	31	7
Si I	6721.84	5.86	-0.94	42.3	7.33	29.1	7.06	38*	4	Ti II	4493.53	1.08	-2.78	34.2	4.90	40.1	5.01	18	7
Ca I	4512.27	2.52	-1.90	25.0	6.33	16.3	5.99	24	5	Ti II	4568.33	1.22	-2.65	32.0	4.84	26.7	4.68	60	7
Ca I	4578.56	2.52	-0.70	85.8	6.33	89.4	6.18	23	5	Ti II	4583.41	1.16	-2.84	31.7	4.96	25.6	4.77	39	7
Ca I	5260.39	2.52	-1.72	33.2	6.32	25.2	6.04	22	5	Ti II	4708.67	1.24	-2.35	51.0	5.02	44.0	4.82	49	7
Ca I	5261.71	2.52	-0.58	98.7	6.49	91.7	6.19	22	5	Ti II	4874.01	3.09	-0.86	36.4	4.91	27.3	4.70	114	7
Ca I	5512.99	2.93	-0.46	83.9	6.36	82.2	6.16	48	5	Ti II	4911.20	3.12	-0.64	51.4	5.11	48.7	5.06	114	7
Ca I	5581.98	2.52	-0.56	94.3	6.38	88.8	6.11	21	5	Ti II	5005.17	1.57	-2.73	23.9	5.02	16.2	4.76	71	7
Ca I	5590.13	2.52	-0.57	93.0	6.37	86.6	6.09	21	5	Ti II	5013.69	1.58	-2.14	49.5	5.08	43.7	4.92	71	7
Ca I	5601.29	2.52	-0.52	102.8	6.47	99.0	6.21	21	5	Ti II	5336.79	1.58	-1.60	72.3	5.09	71.0	5.03	69	7
Ca I	6102.73	1.88	-0.81	122.3	6.10	123.8	5.86	3	5	Ti II	5418.77	1.58	-2.13	48.7	5.02	41.3	4.83	69	7
Ca I	6166.44	2.52	-1.14	72.3	6.37	64.2	6.08	20	5	V I	4437.84	0.29	-0.71	37.1	4.03	32.9	3.76	21	8
Ca I	6169.04	2.52	-0.80	93.5	6.34	90.8	6.09	20	5	V I	4577.18	0.00	-1.08	33.6	4.01	36.5	3.91	4	8
Ca I	6169.56	2.52	-0.48	114.0	6.26	109.4	5.98	20	5	V I	5727.06	1.08	-0.02	38.7	4.04	–	–	35	8
Ca I	6455.60	2.52	-1.34	56.7	6.39	47.3	6.09	19	5	V I	6119.53	1.06	-0.36	22.1	3.93	21.8	3.78	34	8
Ca I	6471.67	2.52	-0.69	89.3	6.35	85.2	6.12	18	5	V I	6243.11	0.30	-0.94	29.6	3.94	29.9	3.78	19	8
Ca I	6493.79	2.52	-0.11	124.4	6.26	116.6	5.95	18	5	Cr I	4545.96	0.94	-1.38	81.6	5.68	80.4	5.43	10	4
Ca I	6499.65	2.52	-0.82	82.5	6.37	81.2	6.19	18	5	Cr I	4616.13	0.98	-1.18	90.3	5.71	83.3	5.34	21	4
Ca I	6572.79	0.00	-4.32	32.1	6.37	33.4	6.24	1	5	Cr I	4626.18	0.97	-1.32	82.2	5.66	72.7	5.24	21	4
Ca I	6717.69	2.71	-0.52	99.5	6.36	98.7	6.04	32	5	Cr I	4646.17	1.03	-0.71	105.5	5.55	94.3	5.11	21	4
Sc I	4023.69	0.02	0.38	57.5	3.12	51.3	2.78	7	6	Cr I	4651.29	0.98	-1.46	82.9	5.82	66.1	5.23	21	4
Sc II	4246.84	0.31	0.24	156.6	3.17	153.8	2.94	7	6	Cr I	4652.17	1.00	-1.03	100.8	5.77	86.3	5.26	21	4
Sc II	5239.82	1.45	-0.76	52.0	3.22	48.7	3.12	26	6	Cr I	4708.02	3.17	0.11	57.5	5.58	41.5	5.11	186	4
Sc II	5526.82	1.77	-0.01	75.1	3.32	65.4	3.06	31	6	Cr I	4718.42	3.19	0.10	64.1	5.74	55.9	5.42	186	4
Sc II	5640.99	1.50	-0.99	39.7	3.18	34.7	3.04	29	6	Cr I	4730.72	3.08	-0.19	48.3	5.67	30.5	5.12	145	4
Sc II	5657.88	1.51	-0.54	66.1	3.36	55.6	3.09	29	6	Cr I	4737.35	3.07	-0.10	55.7	5.68	43.0	5.26	145	4
Sc II	5667.15	1.50	-1.21	32.1	3.22	26.1	3.05	29	6	Cr I	4756.12	3.10	0.09	62.9	5.76	52.3	5.39	145	4
Sc II	5669.04	1.50	-1.10	34.1	3.16	29.7	3.03	29	6	Cr I	4936.34	3.11	-0.34	46.2	5.77	37.6	5.46	166	4
Ti I	4060.27	1.05	-0.69	37.8	4.82	44.5	4.83	80	7	Cr I	4964.93	0.94	-2.53	37.7	5.65	33.3	5.40	9	4
Ti I	4186.13	1.50	-0.24	42.7	4.91	43.7	4.79	129	7	Cr I	5247.57	0.96	-1.63	82.0	5.78	74.5	5.42	18	4
Ti I	4287.41	0.84	-0.37	75.3	5.20	76.7	5.01	44	7	Cr I	5296.70	0.98	-1.41	91.9	5.77	80.7	5.33	18	4
Ti I	4453.32	1.43	-0.03	64.5	5.16	–	–	113	7	Cr I	5300.75	0.98	-2.13	58.6	5.75	44.0	5.25	18	4
Ti I	4465.81	1.74	-0.13	40.9	4.95	40.7	4.81	146	7	Cr I	5345.81	1.00	-0.98	116.8	5.73	111.0	5.37	18	4
Ti I	4512.74	0.84	-0.40	67.5	4.99	68.4	4.82	42	7	Cr I	5348.33	1.00	-1.29	99.5	5.79	86.5	5.32	18	4
Ti I	4518.03	0.83	-0.25	73.0	4.97	74.6	4.80	42	7	Cr I	5787.93	3.32	-0.08	45.7	5.62	32.3	5.22	188	4
Ti I	4534.79	0.84	0.35	95.9	4.86	96.5	4.60	42	7	Cr II	4588.20	4.07	-0.65	71.8	5.69	59.4	5.40	44	9
Ti I	4548.77	0.83	-0.28	70.9	4.95	82.8	4.99	42	7	Cr II	5237.32	4.07	-1.17	53.0	5.75	39.2	5.42	43	9
Ti I	4555.49	0.85	-0.40	63.1	4.89	64.5	4.74	42	7	Cr II	5305.87	3.83	-1.91	24.6	5.48	13.2	5.13	24	9
Ti I	4617.28	1.75	0.44	63.7	4.94	61.3	4.72	145	7	Mn I	4055.55	2.14	-0.08	125.5	5.76	107.2	5.26	5	10
Ti I	4623.10	1.74	0.16	56.6	5.03	52.7	4.79	145	7	Mn I	4082.94	2.18	-0.36	91.3	5.60	76.6	5.07	5	10
Ti I	4639.36	1.74	-0.05	43.2	4.90	49.4	4.91	145	7	Mn I	4451.59	2.89	0.28	95.1	5.55	80.0	5.06	22	10
Ti I	4639.66	1.75	-0.14	43.5	5.01	44.4	4.89	145	7	Mn I	4470.14	2.94	-0.44	56.9	5.46	36.7	4.82	22	10
Ti I	4656.47	0.00	-1.28	68.8	5.07	76.2	5.05	6	7	Mn I	4502.22	2.92	-0.34	59.6	5.41	43.1	4.86	22	10
Ti I	4722.61	1.05	-1.47	18.3	5.02	18.7	4.88	75	7	Mn I	4709.72	2.89	-0.49	68.4	5.73	44.9	5.01	21	10
Ti I	4742.80	2.24	0.21	31.6	4.85	32.5	4.74	233	7	Mn I	4739.11	2.94	-0.61	59.3	5.66	38.7	5.01	21	10
Ti I	4758.12	2.25	0.51	44.9	4.87	39.8	4.63	233	7	Mn I	4765.86	2.94	-0.09	77.4	5.57	66.0	5.15	21	10
Ti I	4759.28	2.25	0.59	44.8	4.79	43.9	4.64	233	7	Mn I	4766.42	2.92	0.10	93.8	5.68	76.3	5.16	21	10
Ti I	4820.41	1.50	-0.38	42.3	4.96	39.9	4.77	126	7	Mn I	4783.42	2.30	0.03	140.1	5.75	121.1	5.27	16	10
Ti I	4885.09	1.89	0.41	62.6	5.04	70.3	5.05	231	7	Mn I	5117.94	3.13	-1.20	24.0	5.51	–	–	32	10
Ti I	4913.62	1.87	0.22	50.6	4.91	48.1	4.71	157	7	Mn I	5432.55	0.00	-3.79	49.6	5.61	25.9	4.86	1	10
Ti I	4981.74	0.85	0.57	119.3	4.92	120.6	4.64	38	7	Mn I	6021.80	3.07	-0.05	96.9	5.85	69.4	5.17	27	10
Ti I	4999.51	0.83	0.32	102.5	4.91	104.8	4.67	38	7	Co I	4121.33	0.92	-0.33	124.0	5.06	113.1	4.61	28	11
Ti I	5009.65	0.02	-2.20	24.2	4.88	34.5	4.95	5	7	Co I	4813.48	3.21	0.12	45.4	5.02	31.1	4.56	158	11
Ti I	5016.17	0.85	-0.48	64.8	4.94	64.6	4.76	38	7	Co I	5301.05	1.71	-1.90	20.6	4.90	–	–	39	11
Ti I	5020.03	0.83	-0.33	77.6	5.07	79.9	4.91	38	7	Co I	5342.71	4.02	0.74	30.5	4.77	21.2	4.43	190	11
Ti I	5022.87	0.83	-0.33	73.2	4.97	73.6	4.78	38	7	Co I	5352.05	3.58	0.06	24.2	4.85	16.6	4.52	172	11
Ti I	5039.96	0.02	-1.08	73.8	4.95	79.9	4.87	5	7	Co I	5483.36	1.71	-1.50	49.8	5.23	39.6	4.84	39	11
Ti I	5064.65	0.05	-0.94	84.8	5.09	87.7	4.92	5	7	Co I	6093.15	1.74	-2.40	9.2	4.95	8.1	4.75	37	11

Table 2 continued

Spec.	λ (Å)	LEP (eV)	log(gf) (dex)	Sun EW (mÅ)	Sun log ϵ(X) (dex)	HD 218209 EW (mÅ)	HD 218209 log ϵ(X) (dex)	RMT	Ref.	Spec.	λ (Å)	LEP (eV)	log(gf) (dex)	Sun EW (mÅ)	Sun log ϵ(X) (dex)	HD 218209 EW (mÅ)	HD 218209 log ϵ(X) (dex)	RMT	Ref.
Ni I	4410.52	3.31	-1.08	57.8	6.39	43.1	5.94	88	4	Ni I	5748.36	1.68	-3.26	28.8	6.26	19.3	5.87	45	4
Ni I	4470.48	3.40	-0.40	79.5	6.24	76.2	5.98	86	4	Ni I	5805.23	4.17	-0.64	40.5	6.30	28.2	5.93	234	4
Ni I	4606.23	3.60	-1.02	48.0	6.37	38.8	6.05	100	4	Ni I	6007.32	1.68	-3.34	25.4	6.24	22.5	6.04	42	4
Ni I	4686.22	3.60	-0.64	62.3	6.30	58.9	6.08	98	4	Ni I	6086.29	4.26	-0.51	43.5	6.30	28.2	5.88	249	4
Ni I	4731.80	3.83	-0.85	45.4	6.35	26.6	5.82	163	4	Ni I	6108.12	1.68	-2.44	65.6	6.30	55.3	5.92	45	4
Ni I	4732.47	4.10	-0.55	44.3	6.29	30.6	5.89	235	4	Ni I	6128.98	1.68	-3.32	25.3	6.21	20.1	5.94	42	4
Ni I	4752.43	3.66	-0.69	59.1	6.33	43.1	5.86	132	4	Ni I	6130.14	4.26	-0.96	21.6	6.24	11.5	5.82	248	4
Ni I	4756.52	3.48	-0.34	77.5	6.19	76.1	5.96	98	4	Ni I	6175.37	4.09	-0.54	50.7	6.32	36.4	5.92	217	4
Ni I	4806.99	3.68	-0.64	61.4	6.35	54.7	6.07	163	4	Ni I	6176.82	4.09	-0.53	63.0	6.54	48.0	6.13	228	4
Ni I	4829.03	3.54	-0.33	80.1	6.24	68.7	5.85	131	4	Ni I	6204.61	4.09	-1.14	21.7	6.26	18.2	6.08	226	4
Ni I	4852.56	3.54	-1.07	44.7	6.28	42.3	6.10	130	4	Ni I	6322.17	4.15	-1.17	18.3	6.24	–	–	249	4
Ni I	4904.42	3.54	-0.17	87.1	6.19	78.1	5.84	129	4	Ni I	6327.60	1.68	-3.15	37.9	6.34	27.8	5.97	44	4
Ni I	4913.98	3.74	-0.62	55.3	6.24	42.3	5.84	132	4	Ni I	6378.26	4.15	-0.90	31.5	6.32	23.5	6.04	247	4
Ni I	4935.83	3.94	-0.36	62.9	6.30	48.5	5.88	177	4	Ni I	6414.59	4.15	-1.21	16.8	6.23	–	–	244	4
Ni I	4946.03	3.80	-1.29	28.0	6.35	17.0	5.96	148	4	Ni I	6482.81	1.93	-2.63	40.8	6.12	31.8	5.79	66	4
Ni I	4953.21	3.74	-0.66	56.2	6.30	40.9	5.85	111	4	Ni I	6598.61	4.23	-0.98	24.7	6.30	–	–	249	4
Ni I	4998.23	3.61	-0.78	57.5	6.33	43.2	5.90	111	4	Ni I	6635.14	4.42	-0.83	24.0	6.31	15.2	5.97	264	4
Ni I	5010.94	3.63	-0.87	48.4	6.23	33.4	5.79	144	4	Ni I	6767.78	1.83	-2.17	79.6	6.47	67.4	6.06	57	4
Ni I	5032.73	3.90	-1.27	23.8	6.31	16.2	6.00	207	4	Ni I	6772.32	3.66	-0.99	48.4	6.27	35.3	5.89	127	4
Ni I	5035.37	3.63	0.29	107.0	6.05	91.5	5.63	143	4	Zn I	4722.16	4.03	-0.39	66.1	4.70	65.0	4.58	2	12
Ni I	5042.19	3.64	-0.57	61.8	6.21	52.6	5.88	131	4	Zn I	4810.54	4.08	-0.17	72.3	4.66	73.6	4.58	2	12
Ni I	5048.85	3.85	-0.37	66.1	6.29	51.5	5.86	195	4	Sr I	4607.34	0.00	0.28	45.4	2.91	32.0	2.28	2	13
Ni I	5082.35	3.66	-0.54	62.5	6.22	55.2	5.92	130	4	Y II	4883.69	1.08	0.07	57.6	2.33	53.4	2.15	22	14
Ni I	5084.10	3.68	0.03	91.1	6.14	78.2	5.75	162	4	Y II	5087.43	1.08	-0.17	48.3	2.25	31.1	1.69	20	14
Ni I	5088.54	3.85	-0.91	31.9	6.12	23.9	5.83	190	4	Zr II	4208.98	0.71	-0.46	44.7	2.68	39.3	2.45	41	15
Ni I	5102.97	1.68	-2.62	48.1	6.16	36.7	5.74	49	4	Ba II	4554.04	0.00	0.14	174.6	2.17	154.7	1.78	1	16
Ni I	5115.40	3.83	-0.11	75.2	6.19	68.9	5.90	177	4	Ba II	5853.69	0.60	-0.91	62.8	2.28	51.2	1.87	2	16
Ni I	5155.13	3.90	-0.66	49.2	6.28	34.5	5.86	206	4	Ba II	6141.71	0.70	-0.03	112.2	2.23	98.9	1.87	2	16
Ni I	5435.87	1.99	-2.60	52.0	6.52	40.0	6.09	70	4	Ba II	6496.91	0.60	-0.41	97.5	2.30	90.6	2.01	2	16
Ni I	5587.87	1.93	-2.14	55.8	6.08	39.7	5.56	70	4	Ce II	4562.37	0.48	0.21	21.9	1.65	18.6	1.47	1	17
Ni I	5593.75	3.90	-0.84	45.4	6.35	28.3	5.88	206	4	Ce II	4628.16	0.52	0.14	18.4	1.63	12.9	1.34	1	17
Ni I	5625.33	4.09	-0.70	38.1	6.24	28.8	5.94	221	4	Nd II	4446.40	0.20	-0.35	12.7	1.41	8.0	1.08	49	18
Ni I	5637.12	4.09	-0.80	33.3	6.23	–	–	218	4	Nd II	5092.80	0.38	-0.61	7.0	1.48	–	–	48	18
Ni I	5641.89	4.10	-1.08	24.6	6.31	13.1	5.87	234	4	Nd II	5293.17	0.82	0.10	10.3	1.39	–	–	75	18
Ni I	5682.21	4.10	-0.47	51.9	6.30	33.9	5.83	232	4	Sm II	4577.69	0.25	-0.65	5.2	0.96	–	–	23	19

References for the adopted gf-values: (1) Takeda et al. (2003), (2) Pehlivan Rhodin et al. (2017), (3) Shi et al. (2011), (4) NIST Atomic Spectra Database (http://physics.nist.gov/PhysRefData/ASD), (5) Den Hartog et al. (2021), (6) Lawler et al. (2019), (7) Lawler et al. (2013), (8) Lawler et al. (2014), (9) Lawler et al. (2017), (10) Den Hartog et al. (2011), (11) Lawler et al. (2015), (12) Biemont & Godefroid (1980), (13) Hansen et al. (2013), (14) Hannaford et al. (1982), (15) Biemont et al. (1981), (16) Klose et al. (2002), (17) Lawler et al. (2009), (18) Den Hartog et al. (2003), (19) Lawler et al. (2006), (†) Bard & Kock (1994), (*) Meléndez & Barbuy (2009)

During the calculation of the model atmosphere, the effect of convection on the reported abundances is also taken into consideration. In one-dimensional (1D) atmosphere modeling, it is currently common practice to assume a universal value of 1.5 for the mixing length parameter (α). However, in order to test the impact of convection on final abundances in this study, the ATLAS models were produced using two different methods for calculating α. Two well known references in the literature, Ludwig et al. (1999) and Magic et al. (2015), for the calculation of α, yields two different values (1.59 and 1.98) even when the same set of model parameters is employed. The logarithmic abundance of ionized iron showed a 0.01 dex increase for the model atmosphere computed with the α parameter set to 1.59 and the model parameters from the ELODIE spectrum. For α = 1.98, it is +0.02 dex. With regards to the FGK dwarf field stars, it is expected that the influence of the mixing length parameter, for instance, on the determination of metallicity would be minimal, amounting to less than 0.02 dex over eight dwarf stars (Song et al. 2020). Thus, our results for HD 218209 confirm those of Song et al. (2020). Regarding the model parameters of HD 218209 from the PolarBASE spectrum, the logarithmic abundance of ionized iron remained the same for the model atmosphere computed with α = 1.59. The difference in logarithmic abundance is 0.02 dex for α = 1.98.

The resulting stellar model parameters for HD 218209 along with our determination of model parameters of the Sun are listed in Table 5. Table 4 lists the model parameters reported for the star in the literature. Rebolo et al. (1988), Abia et al. (1988), and Kim et al. (2016) show the largest variations compared to our log g. The abundances obtained for the Solar photosphere as a result of the Solar analysis are given in Table 3. The Solar abundances from Asplund et al. (2009) are also included for comparison. In Table 3, we provide a summary of element abundances based on LTE-based model parameters. log ϵ is the logarithm of the abundances. The errors reported in log ϵ abundances are the 1σ line-to-line scatter in abundances. [X/H] is the logarithmic abundance ratio of hydrogen to the corresponding Solar value, and [X/Fe] is the logarithmic abundance considering the Fe I abundance. The error in [X/Fe] is the square root of the sum of the quadratures of the errors in [X/H] and [Fe/H]. Table 3 also presents the abundances obtained using the PolarBase spectrum of the star as [X/Fe] ratio.

Table 3. Solar abundances obtained by employing the Solar model atmosphere from Castelli & Kurucz (2003) compared to the photospheric abundances from Asplund et al. (2009). The abundances were calculated using the line EWs.

Species	HD 218209				Sun[†]		Asplund et al. (2009)	
	log ϵ(X)[1] (dex)	[X/Fe][1] (dex)	[X/Fe][2] (dex)	N^1	log $\epsilon_\odot$(X)	N	log $\epsilon_\odot$(X) (dex)	Δ log $\epsilon_\odot$(X)
Na I	5.79±0.09	-0.02±0.14	0.00±0.18	2	6.16±0.07	2	6.24±0.04	0.08
Mg I	7.48±0.06	0.23±0.13	0.09±0.20	2	7.60±0.08	2	7.60±0.04	0.00
Si I	7.28±0.09	0.13±0.14	0.13±0.19	11	7.50±0.07	12	7.51±0.03	0.01
Ca I	6.09±0.10	0.10±0.15	0.10±0.19	18	6.34±0.08	18	6.34±0.04	0.00
Sc I	2.78±0.00	0.01±0.08	-0.33±0.14	1	3.12±0.00	1	3.15±0.04	0.03
Sc II	3.05±0.06	0.17±0.13	0.18±0.20	7	3.23±0.08	7	3.15±0.04	0.08
Ti I	4.82±0.12	0.21±0.17	0.21±0.21	39	4.96±0.09	43	4.95±0.05	0.01
Ti II	4.86±0.13	0.22±0.17	0.18±0.19	12	4.99±0.08	12	4.95±0.05	0.04
V I	3.81±0.07	0.17±0.12	0.05±0.15	4	3.99±0.05	5	3.93±0.08	0.06
Cr I	5.30±0.11	-0.06±0.15	-0.01±0.18	19	5.71±0.07	19	5.64±0.04	0.07
Cr II	5.32±0.16	0.03±0.23	-0.01±0.20	3	5.64±0.14	3	5.64±0.04	0.00
Mn I	5.06±0.15	-0.21±0.21	-0.23±0.23	12	5.62±0.13	13	5.43±0.05	0.19
Fe I	7.17±0.12	-0.02±0.17	-0.01±0.20	128	7.54±0.09	132	7.50±0.04	0.04
Fe II	7.16±0.07	0.00±0.11	0.00±0.19	15	7.51±0.04	17	7.50±0.04	0.01
Co I	4.62±0.15	0.00±0.23	0.03±0.26	6	4.97±0.15	7	4.99±0.07	0.02
Ni I	5.91±0.12	-0.02±0.17	-0.03±0.21	50	6.28±0.09	54	6.22±0.04	0.06
Zn I	4.58±0.01	0.25±0.09	0.26±0.17	2	4.68±0.03	2	4.56±0.05	0.12
Sr I	2.28±0.00	-0.28±0.08	-0.16±0.14	1	2.91±0.00	1	2.87±0.07	0.04
Y II	1.92±0.32	-0.02±0.33	-0.15±0.22	2	2.29±0.05	2	2.21±0.05	0.08
Zr II	2.45±0.00	0.12±0.08	0.27±0.14	1	2.68±0.00	1	2.58±0.04	0.10
Ba II	1.88±0.09	-0.01±0.13	0.06±0.20	4	2.24±0.06	4	2.18±0.09	0.06
Ce II	1.40±0.09	0.11±0.12	0.25±0.21	2	1.64±0.02	2	1.58±0.04	0.06
Nd II	1.08±0.00	0.01±0.09	0.19±0.14	1	1.42±0.05	3	1.42±0.04	0.00
Sm II	–	–	–	–	0.96±0.00	1	0.96±0.04	0.00

(1) The abundances are obtained using the ELODIE spectrum. (2) The abundances are obtained using the PolarBASE spectrum. (*) $\Delta\log\epsilon_\odot(X) = \log\epsilon_\odot(X)_{\rm This\ study} - \log\epsilon_\odot(X)_{\rm Asplund}$. (†) The Solar abundances calculated in this study.

Table 4. Atmospheric parameters of HD 218209 from this study.

$T_{\rm eff}$ (K)	log g (cgs)	[Fe/H] (dex)	Notes
5650	4.55	-0.37	This study (ELODIE)
5630	4.43	-0.32	This study (PolarBASE)
5506	4.38	-0.46	Takeda (2023)
5636	4.56	-0.47	Rice & Brewer (2020)
5518	4.39	-0.49	Aguilera-Gómez et al. (2018)
5623	4.46	-0.40	Luck (2017)
5555	4.26	-0.49	Boeche & Grebel (2016)
5565	4.29	-0.49	Boeche & Grebel (2016)
5669	4.24	-0.39	Kim et al. (2016)
5575	4.11	-0.46	Kim et al. (2016)
5607	4.07	-0.58	Kim et al. (2016)
5536	4.37	-0.46	Da Silva et al. (2015)
5705	4.50	-0.43	Mishenina et al. (2015)
5705	4.50	-0.43	Mishenina et al. (2013)
5592	4.25	-0.51	Lee et al. (2011)
5592	4.33	-0.61	Lee et al. (2011)
5592	4.31	-0.65	Lee et al. (2011)
5705	4.50	-0.43	Mishenina et al. (2011)
5539	4.37	-0.50	Da Silva et al. (2011)
5600	–	–	Casagrande et al. (2011)
5473	4.57	-0.64	Sozzetti et al. (2009)
5506	4.38	-0.46	Takeda et al. (2007)
5693	–	–	Masana et al. (2006)
5585	4.60	-0.46	Valenti & Fischer (2005)
5684	–	–	Kovtyukh et al. (2004)
5705	4.50	-0.43	Mishenina et al. (2004)
5665	4.40	-0.60	Gehren et al. (2004)
5478	4.00	-0.60	Rebolo et al. (1988)
5478	4.00	-0.60	Abia et al. (1988)

Table 5. Model atmosphere parameters for HD 218209 and the Sun.

Star	$T_{\rm eff}$ (K)	log g (cgs)	[Fe/H] (dex)	ξ (km s^{-1})
HD 218209[†]	5650^{+85}_{-85}	$4.55^{+0.13}_{-0.13}$	$-0.35^{+0.07}_{-0.07}$	$0.60^{+0.50}_{-0.50}$
HD 218209[*]	5630^{+145}_{-145}	$4.43^{+0.24}_{-0.24}$	$-0.31^{+0.13}_{-0.13}$	$0.35^{+0.50}_{-0.50}$
Sun	5790^{+45}_{-45}	$4.40^{+0.09}_{-0.09}$	$0.00^{+0.04}_{-0.04}$	$0.66^{+0.50}_{-0.50}$

(†) The ELODIE spectrum was used.
(*) The PolarBase spectrum was used.

4. SUMMARY AND CONCLUSION

We present a line list that can be useful for abundance analysis of G-type stars over 4080 – 6780 Å wavelength region (i.e. for spectra from the ELODIE/SOPHIE library). The line list is expected to be useful for the surveys/libraries with overlapping spectral regions (e.g. ELODIE library, UVES-580 setting of *Gaia*-ESO, and, especially, for the analysis of F- and G-type stars in general). We identified 363 lines of 24 species that have accurate gf-values and are free of blends in the spectra of the Sun and a Solar analogue star, HD 218209. It should be noted that the GES line list does not contain any atomic transitions below 4200 Å and unlike the GES line list, the line list created in this study contains additional four Fe I, one Fe II, 1 Sc I, 2 Ti I and 1 Co I line below this limit. To assess the uncertainty in log gf-values and to minimise systematic errors, we calculated Solar abundances using stellar lines and the high-resolution

KPNO spectrum of the Sun. For the creation of the line list in this study, high resolution and high signal to noise ELODIE spectrum of HD 218209 was used. During the comparison with the GES line list, discrepancies in the $\log gf$ values of some ions were detected. For example, the average difference in $\log gf$ values for 5 V I lines was 0.325±0.328 dex. Similarly, for 11 Mn I lines, the difference was 0.288±0.283 dex. The largest difference detected was 0.585±0.161 dex over 6 Co I lines. For the other elements reported in the new line list presented in this study, the $\log gf$ difference was less than 0.1 dex.

To verify the accuracy of the model parameters obtained for HD 218209 from the ELODIE spectrum, we analyzed the PolarBASE spectrum of the same star. The model parameters from both spectra matched quite well, taking into account the error margins. The element abundances obtained from both spectra also matched quite well, except for Sc I which was represented by a single line at 4023.69 Å in both spectra. The logarithmic abundance from this line in the ELODIE spectrum showed a 0.3 dex increase. Additionally, three other species (Sr I, Zr II, and Ce II), with the latter two presented by two transitions in the spectra, had discrepancies in their logarithmic abundances at around 0.2 dex level. Although the PolarBASE spectrum had higher resolution than the ELODIE spectrum, several lines in the PolarBASE did not have clear line profiles. Unfortunately, there was only one spectrum available in the PolarBASE archive, so a more thorough analysis is recommended to check the abundances of the star from the PolarBASE spectrum.

The model parameters obtained for HD 218209 clearly indicate a Solar analogue character for the star. Although no definite classification scheme exists, Solar analogue stars are defined as the dwarf stars of early G-type which have properties analogous to the Sun (e.g. differences in $T_{\rm eff}$ and $\log g$ are $\pm \leq$ 100–200 K and $\pm \leq$ 0.1–0.2 dex). Indeed, seeing the star listed in a recent study by Takeda (2023) as a Solar analogue was not surprising for us. The model parameters ($T_{\rm eff}$ = 5506 K, $\log g$ = 4.38 cgs, [Fe/H]=-0.46 dex, ξ = 0.74 km s^{-1}) reported by Takeda (2023) are in good agreement with those obtained in this study. However, we report up-to-date abundances for the star using 24 species identified in both ELODIE and PolarBase spectra of the star.

HD 218209 is listed in *Gaia* DR2 (Gaia Collaboration et al. 2018) with *Gaia* DR2 2213415145505277824 designation and a $T_{\rm eff}$ of 5648 K. The surface gravity and metallicity of the star were not reported. HD 218209 is also listed in the *Gaia* DR3 (Gaia Collaboration et al. 2023). Our spectroscopic measurements of the temperature and surface gravity of the star align very well with the values reported by the *Gaia* consortium, which are $T_{\rm eff}$ = 5528 K and $\log g$ = 4.40 cgs. However, there seems to be an error in the reported metallicity of the star by *Gaia*, which states [Fe/H] = -0.79 dex. This discrepancy is likely due to the incorrect selection of the template spectrum for the star in the *Gaia* DR3, where the metallicity of the template star is reported as -0.50 dex.

In the *Gaia* DR3 (Gaia Collaboration et al. 2023), an important addition is a collection of 220 million low-resolution BP/RP spectra. The GSP-Phot catalogue provides consistent estimations of stellar parameters for 471 million sources with G < 19 mag, derived from the BP/RP spectra, parallax, and integrated photometry. It assumes that each source is a single star and that any intrinsic time variability is lost when using combined BP/RP spectra. However, it is important to note that the GSP-Phot results from the BP/RP spectra in the *Gaia* DR3 may still be affected by systematic effects, particularly in the [M/H] estimates with large systematic errors. Consequently, it is advised not to rely on these estimates as they can only provide qualitative information at best (Beck et al. 2023).

In a study of stellar and sub-stellar companions of nearby stars from the *Gaia* DR2 (Gaia Collaboration et al. 2018), Kervella et al. (2019) examined the status of stars exhibiting anomalies in their proper motions as binary stars. HD 218209 as a high proper-motion star happens to be one of the common stars. The study found no evidence of a companion around HD 218209, even at distances ranging from 1 to 50 astronomical units (au) and down to planetary masses. Therefore, the authors concluded that HD 218209 is a single star (P. Kervella, private communication, 2023).

Soubiran & Girard (2005), in their exploration of abundance discrepancies between the thin disc and thick disc of the Galaxy, identified HD 218209 out of the 44 stars as being part of the Hercules stream with a probability of 0.76. The Hercules stream shares chemical characteristics with the thin disc, which bolsters the dynamic hypothesis (i.e. the influence of the central bar of the Galaxy impacting stars) of its origin. However, kinematic and orbital dynamics analysis for the star is the subject of another study.

Peer Review: Externally peer-reviewed.

Author Contribution: Conception/Design of study - T.Ş., S.B.; Data Acquisition - T.Ş., M.M., N.Ç.; Data Analysis/Interpretation - T.Ş., S.B., M.M., N.Ç.; Drafting Manuscript - T.Ş.; Critical Revision of Manuscript - T.Ş., S.B., M.M., N.Ç; Final Approval and Accountability - T.Ş., S.B., M.M., N.Ç.

Conflict of Interest: Authors declared no conflict of interest.

Financial Disclosure: This study has partly been supported by the Scientific and Technological Research Council (TÜBİTAK) MFAG-121F265.

Acknowledgements: We thank Ferhat GÜNEY for his help with the preparation of Figure 2. We also thank Gizay YOLALAN and Sena A. ŞENTÜRK for helpful discussion.

Note: The Co-Editor-in-Chief was not involved in the evaluation, peer-review and decision processes of the article. These processes were carried out by the Editor-in-Chief and the member editors of the editorial management board.

LIST OF AUTHOR ORCIDS

T. Şahin https://orcid.org/0000-0002-0296-233X
M. Marışmak https://orcid.org/0000-0002-9397-2778
N. Çınar https://orcid.org/0000-0002-5155-9280
S. Bilir https://orcid.org/0000-0003-3510-1509

REFERENCES

Abia C., Rebolo R., Beckman J. E., Crivellari L., 1988, A&A, 206, 100

Aguilera-Gómez C., Ramírez I., Chanamé J., 2018, A&A, 614, A55

Allende Prieto C., et al., 2008, Astronomische Nachrichten, 329, 1018

Asplund M., Grevesse N., Sauval A. J., Scott P., 2009, ARA&A, 47, 481

Bard A., Kock M., 1994, A&A, 282, 1014

Beck P. G., et al., 2023, arXiv e-prints, p. arXiv:2307.10812

Biemont E., Godefroid M., 1980, A&A, 84, 361

Biemont E., Grevesse N., Hannaford P., Lowe R. M., 1981, ApJ, 248, 867

Boeche C., Grebel E. K., 2016, A&A, 587, A2

Casagrande L., Schönrich R., Asplund M., Cassisi S., Ramírez I., Meléndez J., Bensby T., Feltzing S., 2011, A&A, 530, A138

Castelli F., Kurucz R. L., 2003, in Piskunov N., Weiss W. W., Gray D. F., eds, Published on behalf of the IAU by the Astronomical Society of the Pacific Vol. 210, Modelling of Stellar Atmospheres. p. A20 (arXiv:astro-ph/0405087), doi:10.48550/arXiv.astro-ph/0405087

Da Silva R., Milone A. C., Reddy B. E., 2011, A&A, 526, A71

Da Silva R., Milone A. d. C., Rocha-Pinto H. J., 2015, A&A, 580, A24

De Silva G. M., et al., 2015, MNRAS, 449, 2604

Den Hartog E. A., Lawler J. E., Sneden C., Cowan J. J., 2003, ApJS, 148, 543

Den Hartog E. A., Lawler J. E., Sobeck J. S., Sneden C., Cowan J. J., 2011, ApJS, 194, 35

Den Hartog E. A., Lawler J. E., Sneden C., Cowan J. J., Roederer I. U., Sobeck J., 2021, ApJS, 255, 27

Gaia Collaboration et al., 2018, A&A, 616, A11

Gaia Collaboration et al., 2023, A&A, 674, A1

Gehren T., Liang Y. C., Shi J. R., Zhang H. W., Zhao G., 2004, A&A, 413, 1045

Gilmore G., et al., 2012, The Messenger, 147, 25

Hannaford P., Lowe R. M., Grevesse N., Biemont E., Whaling W., 1982, ApJ, 261, 736

Hansen C. J., Bergemann M., Cescutti G., François P., Arcones A., Karakas A. I., Lind K., Chiappini C., 2013, A&A, 551, A57

Heijmans J., et al., 2012, in McLean I. S., Ramsay S. K., Takami H., eds, Society of Photo-Optical Instrumentation Engineers (SPIE) Conference Series Vol. 8446, Ground-based and Airborne Instrumentation for Astronomy IV. p. 84460W, doi:10.1117/12.925806

Heiter U., Jofré P., Gustafsson B., Korn A. J., Soubiran C., Thévenin F., 2015, A&A, 582, A49

Kervella P., Arenou F., Mignard F., Thévenin F., 2019, A&A, 623, A72

Kim B., An D., Stauffer J. R., Lee Y. S., Terndrup D. M., Johnson J. A., 2016, ApJS, 222, 19

Klose J. Z., Fuhr J. R., Wiese W. L., 2002, Journal of Physical and Chemical Reference Data, 31, 217

Kovtyukh V. V., Soubiran C., Belik S. I., 2004, A&A, 427, 933

Kurucz R. L., Furenlid I., Brault J., Testerman L., 1984, Solar flux atlas from 296 to 1300 nm

Lawler J. E., Den Hartog E. A., Sneden C., Cowan J. J., 2006, ApJS, 162, 227

Lawler J. E., Sneden C., Cowan J. J., Ivans I. I., Den Hartog E. A., 2009, ApJS, 182, 51

Lawler J. E., Guzman A., Wood M. P., Sneden C., Cowan J. J., 2013, ApJS, 205, 11

Lawler J. E., Wood M. P., Den Hartog E. A., Feigenson T., Sneden C., Cowan J. J., 2014, ApJS, 215, 20

Lawler J. E., Sneden C., Cowan J. J., 2015, ApJS, 220, 13

Lawler J. E., Sneden C., Nave G., Den Hartog E. A., Emrahoğlu N., Cowan J. J., 2017, ApJS, 228, 10

Lawler J. E., Hala Sneden C., Nave G., Wood M. P., Cowan J. J., 2019, ApJS, 241, 21

Lee Y. S., et al., 2011, AJ, 141, 90

Luck R. E., 2017, AJ, 153, 21

Ludwig H.-G., Freytag B., Steffen M., 1999, A&A, 346, 111

Magic Z., Weiss A., Asplund M., 2015, A&A, 573, A89

Martell S. L., et al., 2017, MNRAS, 465, 3203

Masana E., Jordi C., Ribas I., 2006, A&A, 450, 735

Meléndez J., Barbuy B., 2009, A&A, 497, 611

Mishenina T. V., Soubiran C., Kovtyukh V. V., Korotin S. A., 2004, A&A, 418, 551

Mishenina T. V., Gorbaneva T. I., Basak N. Y., Soubiran C., Kovtyukh V. V., 2011, Astronomy Reports, 55, 689

Mishenina T. V., Pignatari M., Korotin S. A., Soubiran C., Charbonnel C., Thielemann F. K., Gorbaneva T. I., Basak N. Y., 2013, A&A, 552, A128

Mishenina T., Gorbaneva T., Pignatari M., Thielemann F. K., Korotin S. A., 2015, MNRAS, 454, 1585

Molaro P., Monai S., 2012, A&A, 544, A125

Moore C. E., Minnaert M. G. J., Houtgast J., 1966, The solar spectrum 2935 A to 8770 A

Pagel B. E. J., Patchett B. E., 1975, MNRAS, 172, 13

Pehlivan Rhodin A., Hartman H., Nilsson H., Jönsson P., 2017, A&A, 598, A102

Petit P., Louge T., Théado S., Paletou F., Manset N., Morin J., Marsden S. C., Jeffers S. V., 2014, PASP, 126, 469

Placco V. M., et al., 2021, ApJ, 912, L32

Rebolo R., Molaro P., Beckman J. E., 1988, A&A, 192, 192

Rice M., Brewer J. M., 2020, ApJ, 898, 119

Shi J. R., Gehren T., Zhao G., 2011, A&A, 534, A103

Sneden C. A., 1973, PhD thesis, University of Texas, Austin

Song N., Alexeeva S., Sitnova T., Wang L., Grupp F., Zhao G., 2020, A&A, 635, A176

Soubiran C., Girard P., 2005, A&A, 438, 139

Soubiran C., Bienaymé O., Siebert A., 2003, A&A, 398, 141

Sozzetti A., Torres G., Latham D. W., Stefanik R. P., Korzennik S. G., Boss A. P., Carney B. W., Laird J. B., 2009, ApJ, 697, 544

Steinmetz M., et al., 2006, AJ, 132, 1645

Takeda Y., 2023, Acta Astron., 73, 35

Takeda Y., Zhao G., Takada-Hidai M., Chen Y.-Q., Saito Y.-J., Zhang H.-W., 2003, Chinese J. Astron. Astrophys., 3, 316

Takeda Y., Kawanomoto S., Honda S., Ando H., Sakurai T., 2007, A&A, 468, 663

Valenti J. A., Fischer D. A., 2005, ApJS, 159, 141

Yanny B., et al., 2009, AJ, 137, 4377

Zhao G., Zhao Y.-H., Chu Y.-Q., Jing Y.-P., Deng L.-C., 2012, Research in Astronomy and Astrophysics, 12, 723

Şahin T., 2017, Turkish Journal of Physics, 41, 367

Şahin T., Bilir S., 2020, ApJ, 899, 41

Şahin T., Lambert D. L., 2009, MNRAS, 398, 1730

Şahin T., Lambert D. L., Klochkova V. G., Tavolganskaya N. S., 2011, MNRAS, 410, 612

Şahin T., Lambert D. L., Klochkova V. G., Panchuk V. E., 2016, MNRAS, 461, 4071